



Science Arts & Métiers (SAM)

is an open access repository that collects the work of Arts et Métiers Institute of Technology researchers and makes it freely available over the web where possible.

This is an author-deposited version published in: <https://sam.ensam.eu>
Handle ID: <http://hdl.handle.net/10985/22217>

To cite this version :

Zeya WANG, Sandra ZIMMER-CHEVRET, François LÉONARD, Gabriel ABBA - Improvement strategy for the geometric accuracy of bead's beginning and end parts in wire-arc additive manufacturing (WAAM) - The International Journal of Advanced Manufacturing Technology - Vol. 118, n°7-8, p.2139-2151 - 2021

Any correspondence concerning this service should be sent to the repository

Administrator : scienceouverte@ensam.eu



Improvement strategy for the geometric accuracy of bead's beginning and end parts in wire-arc additive manufacturing (WAAM)

Zeya Wang¹  · Sandra Zimmer-Chevret² · François Léonard¹ · Gabriel Abba¹

Received: 23 June 2021 / Accepted: 9 September 2021

© The Author(s), under exclusive licence to Springer-Verlag London Ltd., part of Springer Nature 2021

Abstract

Cold metal transfer (CMT)-based wire-arc additive manufacturing (WAAM) is a promising method for the production of large-scale and complex metallic parts because of its high efficiency, less heat input and low cost. However, a critical and common problem with the arc welding processes is the irregular geometry at the beginning and end parts of the bead due to the ignition and extinction of the arc. Based on experimental investigations of the irregularities and different possible optimization methods, an improvement strategy consisting of configurations with a varying travel speed and an extra return path is presented in this paper. Experimental results show that this strategy can effectively enhance the geometric accuracy at the beginning and end parts of different single beads. In the manufacturing of a thin-wall part and a multi-pass cladding, the improvement of geometric accuracy has also been achieved by this strategy.

Keywords Improvement strategy · Bead start · Bead end · Bead geometric accuracy · WAAM · GMAW

1 Introduction

Wire-arc additive manufacturing (WAAM) is increasingly popular for the low-cost and rapid manufacture of large and complex metallic components due to its high deposition rate and material efficiency [1, 2]. Cold metal transfer (CMT) is a modified gas metal arc welding (GMAW) process which provides a controlled material deposition mode through its innovative wire feed and digital control system [3, 4]. Because of its low heat input and nearly zero spatter [5], the application of CMT in WAAM has gained a lot of attention. Ayarkwa et al. [6] have investigated the effect of the process parameters of CMT in aluminum WAAM and found that the key factor for wall dimensions is the ratio of the wire feed speed (WFS) to the travel speed (TS). Ali et al. [7] analyzed the influence of the arc energy and the thermal field on the resulting mechanical properties and microstructure of the

hot work tool steel in CMT-based WAAM. In [8], different wire electrodes were tested to study the influence of the composition of the filler metal on the thin-wall parts of a nickel alloy made by CMT.

For WAAM systems, it is important to achieve not only an efficient production but also a high geometric accuracy of the fabricated parts [9, 10]; thus, many studies have been conducted to increase the geometric accuracy of the process. Based on a thermally scanned material deposition control method, Kwak and Doumanidis [11] investigated the regulation of the bead width in GMAW-based WAAM. In order to improve the stability of the layer height in the process, Xiong and Zhang [12] designed an adaptive control system to maintain constant the distance between the nozzle and the top surface. Zhao et al. [13] proposed a unit block-based process planning strategy to improve the surface accuracy in WAAM for a complex shell-shaped component. In [14], subtractive manufacturing was integrated with WAAM for better accuracy of the geometry. Meanwhile, dimensional irregularities at the beginning and end parts of the weld bead degrade the final geometric accuracy of the WAAM parts and lead to more material being removed in post-processing, especially for the WAAM multi-layer depositions, where the accumulated geometric errors were demonstrated to become very significant [15].

✉ Zeya Wang
zeya.wang@univ-lorraine.fr

¹ Université de Lorraine, Arts et Metiers Institute of Technology, LCFC, HESAM Université, F-57070 Metz, France

² Arts et Metiers Institute of Technology, Université de Lorraine, LCFC, HESAM Université, F-57070 Metz, France

The accumulation of excessive material in the arc ignition phase results in a hump at the beginning of the weld bead, while a crater at the end of the bead would be formed due to the lack of melted material in the arc extinction phase. Therefore, improvement strategies should be developed to deal with the geometric irregularities at the beginning and end parts of beads [16]. An effective strategy can be significantly useful for the WAAM multi-layer depositions in reducing accumulated geometric errors, it can also be applied in the classical arc welding processes (e.g., cladding) for a more regular geometry [17]. However, in the field of WAAM research, few solutions to this problem have been reported. Considering the geometric instability at the beginning and end parts of the bead, Ding et al. [18] proposed a more continuous planning of the deposition path to avoid frequent arc ignitions and extinctions. Xiong et al. [19] enhanced the process stability by applying a vision-sensing and bead geometry control system in GMAW-based WAAM, but the system was not able to improve the geometric accuracy at the beginning and the end parts of the deposited beads. Similarly, in laser metal wire deposition, Heralić et al. [20] developed an on-line control system to optimize the regularity of the width and height of the bead, while hand-tuned sequences were used instead of the proposed controller at the beginning and end parts of the bead.

In this paper, three different optimization methods, (1) a special 2-step mode of CMT, (2) varying TS configurations, and (3) an extra return path, will be introduced first (Sections 3.1–3.3) and then investigated in experiments to address the dimensional irregularities at the beginning

and end parts of single beads (Sections 4.1–4.3). Based on the experimental results, the optimal method for the beginning part (varying TS configurations) and the most effective method for the end part (extra return path) are selected and combined to build a complete improvement strategy. With different combinations of process parameters tested, the strategy is demonstrated to effectively enhance the geometric accuracy at the beginning and end parts of different single beads (Section 4.4). Furthermore, the strategy is applied in the manufacturing of a thin-wall part and a multi-pass cladding, and their geometric accuracy is also improved (Section 4.5).

2 Experimental setup

Figure 1 shows a schematic diagram of the experimental setup. The robot control cabinet connects a CMT welding power source (Fronius TPS320i) and an ABB IRB8700 robot. Based on the program input from an external computer, the control cabinet coordinates both the motions of the robot and the CMT process. With the mounted welding torch, the robot is used to implement the deposition path. The material of the consumable wire electrode is the high strength steel ER100 (according to American Welding Society (AWS) Standards A5.28 or G 69 6 M21 Mn4Ni1.5CrMo according to ISO 16834) with a diameter of 1.2 mm. The nominal chemical composition of the wire (in wt.%) is provided in Table 1. It should be noticed that the deposit composition also depends on the dilution and reaction gas-pool, thus a variation of the deposited

Fig. 1 Schematic diagram of the experimental setup

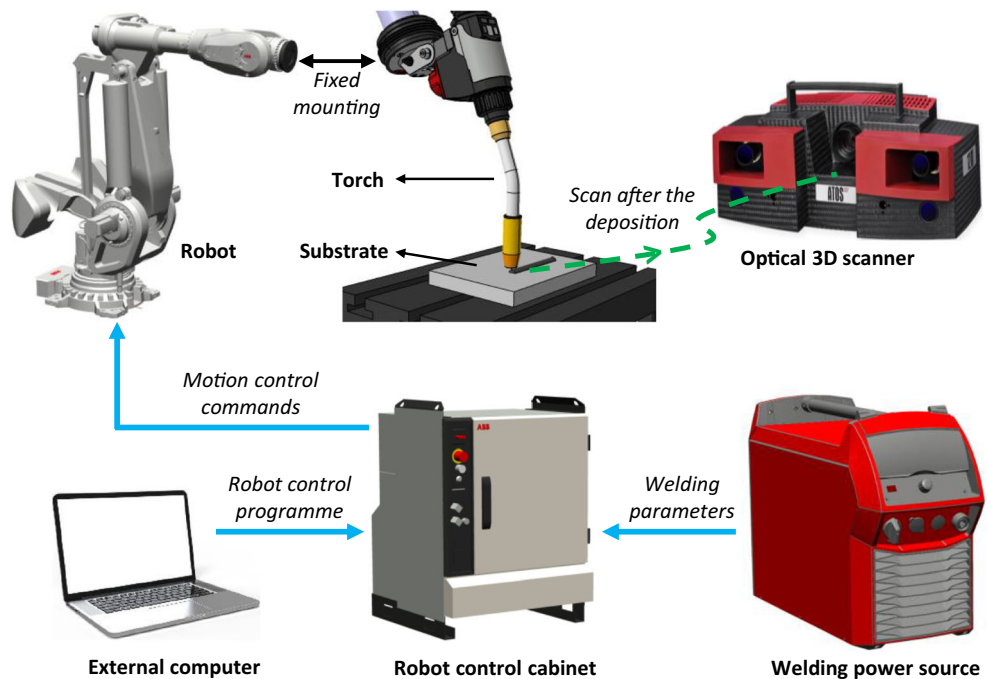


Table 1 Nominal chemical composition of the wire material ER100

Element	C	Si	Mn	Cr	Ni	Mo	P	S	V	Ti	Zr	Al	Cu	Fe
wt. %	0.08	0.54	1.66	0.25	1.58	0.47	0.007	0.01	0.002	0.05	0.001	0.002	0.14	Bal.

material's composition is expected during the fabrication. A gas mixture of Ar (85%) and CO₂ (15%) with a flow rate of 18 L/min is used for shielding. Weld beads are deposited on the substrate, which is made of mild steel S235, 200 mm long, 150 mm wide, and a height of 20 mm. Before the deposition, the substrate is sandblasted to remove the oxides and to maintain a good and consistent surface quality. During the deposition process, the torch is held perpendicular to the substrate, and the nozzle-to-plate distance is kept at 15 mm. The deposited beads will be sandblasted again for the measurement by an optical 3D scanner (ATOS Triple Scan), which is employed to measure quickly and accurately the deposited beads' geometry. Figure 2 presents a typical cross-sectional profile of a weld bead; the two geometric parameters width (W) and height (H) are taken to characterize the geometry of the bead.

3 Methodology

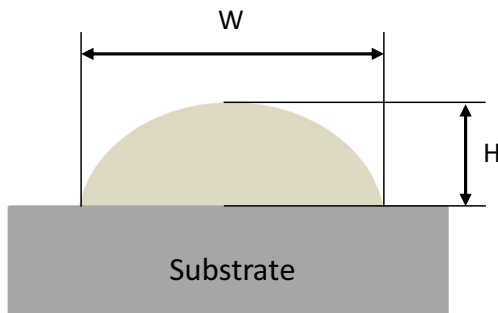
Figure 3 shows a typical weld bead deposited by the standard mode of CMT (without improvement strategy, WFS = 7.5 m/min, TS = 13 mm/s), and a 3D scan of its beginning and end parts. At the beginning part, TS increases from zero to the standard value and the welding source takes more power than steady state to initiate the arc, so that more material is melted and deposited. Moreover, the beginning part has poor wetting on the substrate because of the substrate's lower temperature, which prevents the deposited material from being well spread. Therefore, the accumulated material at the beginning part produces a hump which is generally higher and wider than the stable middle part (Fig. 3a). At the end part, the arc and wire feed are terminated, during which the behavior of the process

varies sharply from moment to moment, thus creating very unsteady temperature and fluid flow fields [21]. Consequently, a slope-shape crater is formed gradually at the end part due to the lesser amount of material being deposited and the flowing of the melted metal (Fig. 3b). Beads with the geometric errors of similar dimensions have also been reported in other studies [6, 22].

In this study, the torch travel distance for each bead deposition is fixed at 100 mm (i.e., the bead's deposition length), and the travel direction is set in the direction of the Y -axis of the coordinate system of the deposition (i.e., $Y = 0$ for the beginning of the path and $Y = 100$ for the end of the path). The overall length of the bead would be slightly greater than 100 mm due to the bead's spreading at the beginning and end of the deposition path. A set of preliminary experiments were carried out to identify the general length of the irregularities at the beginning and end of the bead, with different process parameters (WFS and TS). Based on the preliminary experiments, the first 15 mm of the torch displacement ($Y \in [0, 15]$) is defined as the beginning part and the last 15 mm was taken as the end part ($Y \in [85, 100]$). Different methods are presented in this section with the goal of reducing the geometric irregularities at the beginning and end parts of the bead (i.e., rendering W and H more uniform). In all experimental tests of the methods, the standard values of the WFS and TS were kept constant ($WFS_s = 7.5$ m/min, $TS_s = 13$ mm/s) in order to compare the resulting improvement in the geometry with the bead deposited by the standard mode of CMT with the same parameters (shown in Fig. 3). It should be noted that in the experiments the actual WFS varies from its set value, this problem cannot be eliminated but is mitigated by keeping the process configuration identical (shielding gas, wire material, nozzle-to-plate distance, substrate's size and its surface treatment). The variation of actual WFS is limited to a small range (set value ± 0.3 m/min) to obtain stable and repeatable depositions with the same set WFS.

3.1 Special 2-step mode of CMT

In the welding source of the CMT, based on the given data (wire material and diameter, welding mode, type of shielding gas), the welding voltage and current parameters are automatically adjusted to their standard values according to the user input WFS to obtain a stable and continuous metal transfer. Meanwhile, welding source of the CMT offers an extra optional special 2-step mode to deal with the

**Fig. 2** Illustration of single bead geometry

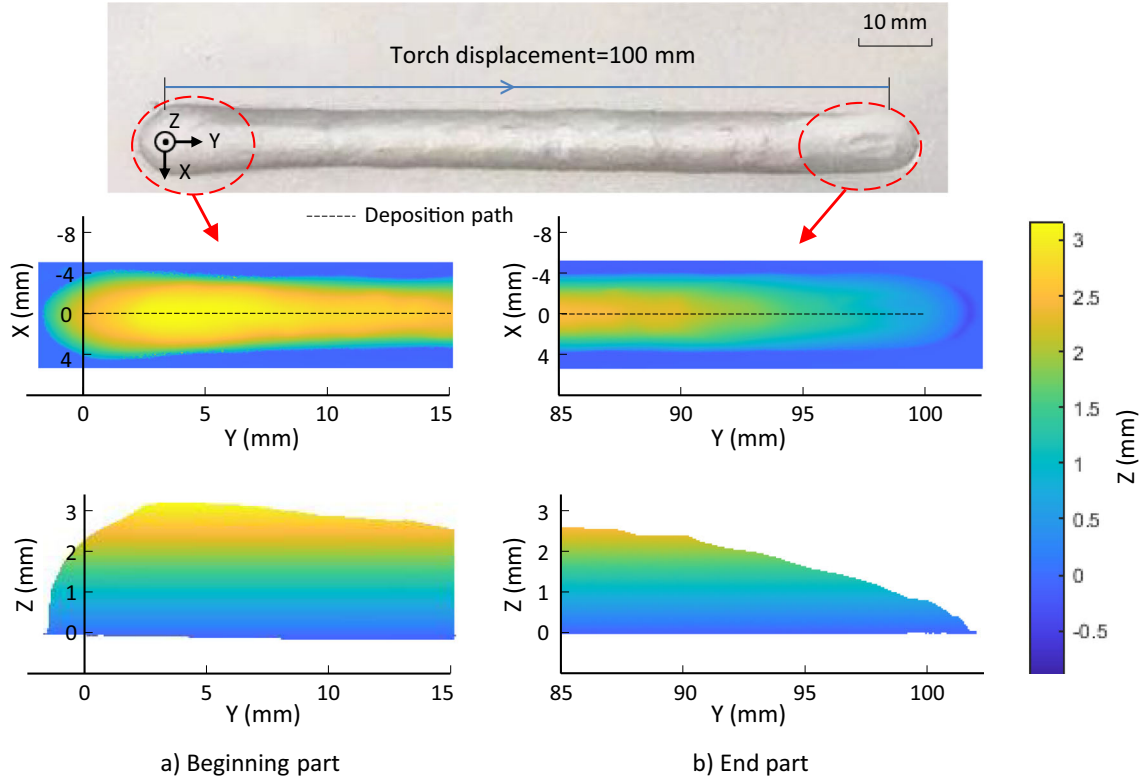


Fig. 3 Geometry of the beginning and end parts of a bead deposited with CMT standard mode ($WFS_s=7.5$ m/min, $TS_s=13$ mm/s)

instabilities at the start and end of the welding, where the current could be set differently from the standard values. Figure 4 gives a comparison of the standard mode of the CMT and the special 2-step mode through a welding current (I)-time (t) diagram. In the special 2-step mode, the beginning welding current (I_b) can be set higher than the standard value (I_s) in percentage (factory setting: $I_b = 135\%I_s$), where more heat is introduced to obtain a better wetting of the bead. Meanwhile, in order not to deposit overly excessive material at the beginning part, the adjustable duration of I_b (t_b) needs to be set short to control

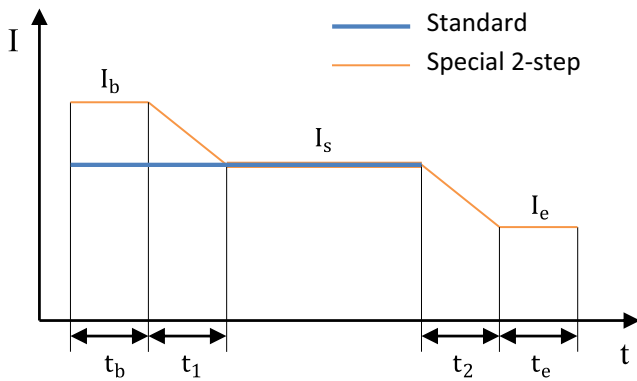


Fig. 4 Comparison of the standard mode of CMT and the special 2-step mode

the heat input ($t_b \leq 0.6$ s in this study). With the same purpose, the transition time from I_b to I_s is fixed at its minimum value: $t_1 = 0.1$ s. At the end of the welding, unlike the immediate disconnection of the power supply in the standard mode, the special 2-step mode maintains a lower end current I_e ($I_e = 50\%I_s$ in the factory setting) for a period of t_e , therefore more material can be deposited at the end of the bead to fill the crater. From I_s to I_e , the linear descent time t_2 is fixed at 0.5 s for a smooth decrease in energy.

In order to test the effectiveness of the special 2-step mode of the CMT in improving the bead geometry at the beginning and end parts, experiments have been carried out with different combinations of I_b (%) and t_b (s) for the beginning part as well as different combinations of I_e (%) and t_e (s) for the end part. Table 2 shows the corresponding experimental data.

3.2 Varying TS configurations

In wire-arc welding, the ratio WFS/TS determines the amount of material deposited per unit length, also known as the area of the cross-section of a single weld bead, as defined in Eq. (1):

$$S = \pi \frac{d_w^2}{4} \times \frac{WFS}{TS} \times \frac{1000}{60} \quad (1)$$

Table 2 Experimental data of the special 2-step mode of CMT

No.	Beginning		End	
	I_b (%)	t_b (s)	I_e (%)	t_e (s)
1	120	0.3	50	0.5
2	135	0.3	65	0.5
3	150	0.3	80	0.5
4	165	0.3	95	0.5
5	120	0.4	50	0.6
6	135	0.4	65	0.6
7	150	0.4	80	0.6
8	165	0.4	95	0.6
9	120	0.5	50	0.7
10	135	0.5	65	0.7
11	150	0.5	80	0.7
12	165	0.5	95	0.7
13	120	0.6	50	0.8
14	135	0.6	65	0.8
15	150	0.6	80	0.8
16	165	0.6	95	0.8

Here, S (mm^2) represents the bead's cross-sectional area and d_w (mm) is the diameter of the metal wire. It can be noted that with WFS (m/min) fixed, varying TS (mm/s) is able to change the bead geometry. Normally, a single bead is always deposited with constant WFS and TS, and the bead's geometric irregularities at the beginning and end parts cannot be compensated for. Therefore, an improvement method through configurations with a TS that varies is proposed as follows: at the beginning of the deposition, TS is decreased from a higher value to the standard value; at the end part, TS is reduced gradually to zero. In this way, the higher TS at the beginning can lead to depositing less material, thus avoiding excessive material accumulation, and the gradual decrease of TS at the end enables more material to be deposited to fill the crater.

Due to the bead's flow and spread before the solidification, varying TS affects not only the bead geometry at the torch's deposition point but also the geometry of the beads nearby. Thus, in order to avoid influencing the stable geometry of the bead's middle part, the zones of the variation of the TS are set to be the first 10 mm and the last 10 mm of the torch displacement, so as to limit the impact to stay within the beginning and end parts. These two distance intervals are determined by the preliminary experimental tests to obtain the optimal improvement performance. The control of the TS is achieved by the command of the robot translation speed: for setting different values of TS, the corresponding displacement vectors of the torch (the robot's tool) have to be specified. Consequently, as illustrated in Fig. 5, the zones of the variation of the TS, at the beginning and end

parts, have each been divided into three smaller sections for the application of different values of TS: $TS_{b1} \geq TS_{b2} \geq TS_{b3}$ for the beginning part, and $TS_{e1} \geq TS_{e2} \geq TS_{e3}$ for the end part. It should be noticed that the illustration figures of TS in this paper do not reflect the robot acceleration and deceleration. Due to the high performance of the robot employed, all acceleration and deceleration in the experiments are realized in less than 0.2s, which have very limited influences on the depositions. The values of TS are set in percentages with respect to the standard value of TS in the middle part (TS_s). Different TS configurations were applied in the experiments to test the performance of geometry improvement. The value of TS for the beginning part varies within the range of [110%, 130%] and at the end part it varies within the range of [25%, 75%]. Table 3 presents the experimental data of the varying TS configurations.

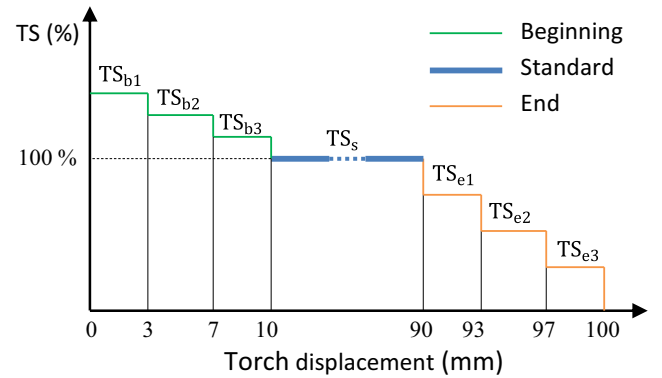
**Fig. 5** Illustration of the varying TS configurations

Table 3 Experimental data of the varying TS configurations

No.	Beginning			End		
	TS_{b1}	TS_{b2}	TS_{b3}	TS_{e1}	TS_{e2}	TS_{e3}
	(%)	(%)	(%)	(%)	(%)	(%)
1	130	130	130	75	75	75
2	130	130	120	75	75	50
3	130	130	110	75	75	25
4	130	120	120	75	50	50
5	130	120	110	75	50	25
6	130	110	110	75	25	25
7	120	120	120	50	50	50
8	120	120	110	50	50	25
9	120	110	110	50	25	25
10	110	110	110	25	25	25

3.3 Extra return path

An extra return path is proposed particularly for dealing with the geometric errors at the end part of the weld bead. By adding a return path after the standard bead deposition (the torch travels a short extra distance in the opposite direction from the end point), this method can deposit additional material more uniformly along the direction of the length of the bead to compensate for the slope-shaped crater. The welding arc has to be extinguished at the end point of the standard deposition path and then reignited at the beginning of the extra return path. Otherwise, if the arc is kept on, in order to switch the direction of movement, the robot's deceleration and reacceleration at the end point will lead to excessive material accumulation and thus increasing the geometric irregularities of the bead. Based on the measurement of the different lengths of the crater of the bead in the preliminary experiments, the extra return distance d_r (mm) is defined as the distance traveled by the torch in 1 s during the standard deposition process (TS_s in mm/s):

$$d_r = TS_s \times 1 \quad (2)$$

It can be seen that the distance interval for the application of this improvement method varies with the parameter TS_s .

Because of the short cooling time, the crater formed will already be at a high temperature before the return path, so it is necessary to reduce the heat input during the return path to keep the deposition process stable and to mitigate the resulting differences in the mechanical properties between the end part and the rest part of the bead. Generally, the WFS of the return path (WFS_r) is set lower than the standard value (WFS_s) and at the same time a higher return TS (TS_r) is applied. Figure 6 illustrates the principle of the method of the extra return path, where WFS_r and TS_r are

expressed in percentages of the standard deposition values. Different combinations of WFS_r and TS_r were tested in the experiments to identify the optimal configuration for the end part's improvement. The experimental data is shown in Table 4.

3.4 The developed improvement strategy

The results of these experimental investigations of the three different methods (which will be presented and discussed in Section 4) show that the varying TS configuration with $TS_{b1}=130\%$, $TS_{b2}=120\%$, and $TS_{b3}=110\%$ is the most effective in reducing the geometric irregularities at the beginning part of the bead, while the extra return path with

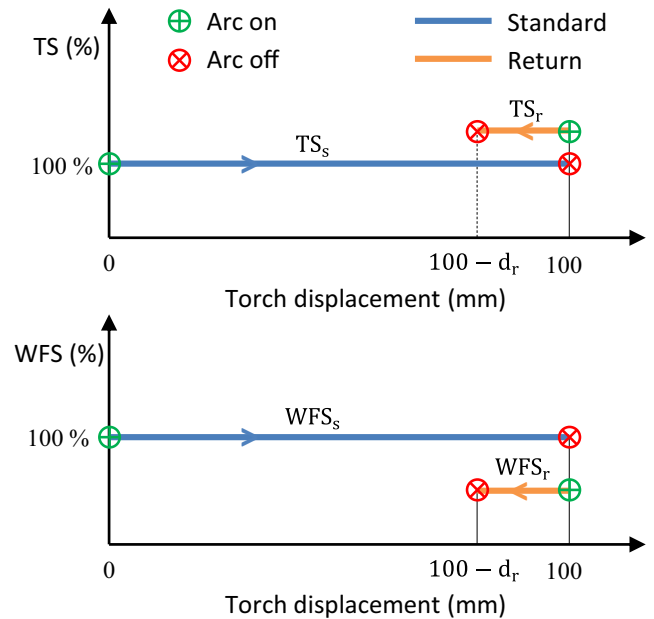
**Fig. 6** Illustration of the extra return path

Table 4 Experimental data of the extra return path

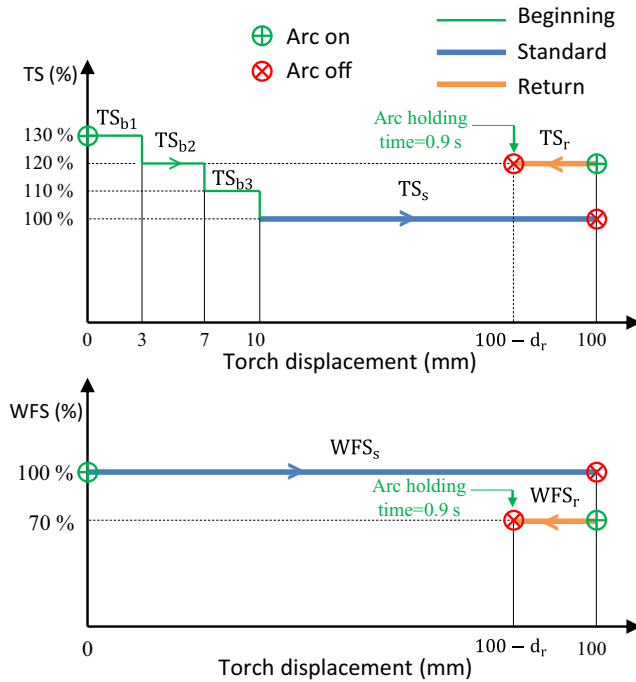
No.	1	2	3	4	5	6	7	8	9	10	11	12	13	14	15	16
TS_r (%)	110	110	110	110	120	120	120	120	130	130	130	130	140	140	140	140
WFS_r (%)	50	60	70	80	50	60	70	80	50	60	70	80	50	60	70	80

$TS_r=120\%$, $WFS_r=70\%$, and an additional arc holding time of 0.9 s at the end of the return path produces the most regular geometry at the end part. Therefore, these two methods are combined as a complete strategy to improve the geometric accuracy at the beginning and end parts of the bead. Figure 7 provides an illustration of the resulting improvement strategy.

4 Results and discussion

Along the length of the deposited bead (in the direction of the Y -axis), the bead's W and H are measured every 0.5 mm through the use of the 3D scanner. In order to analyze the geometric accuracy of the beginning and end parts of the bead, the index E_m (%) is introduced to calculate in percentage the mean error between the stable W or H of the middle part and the W or H measured at the beginning/end part:

$$E_m = \frac{1}{N} \sum_{i=1}^N \left(\frac{|X_i - \bar{X}_{middle}|}{\bar{X}_{middle}} \right) \times 100\% \quad (3)$$

**Fig. 7** Illustration of the developed improvement strategy

Here, N represents the number of measurements of W or H at the beginning/end part, X_i (mm) is the measured value of W or H , and \bar{X}_{middle} (mm) is the mean value of W or H at the middle part (\bar{W}_{middle} , \bar{H}_{middle}). Figure 8 shows the measurement results of the beginning and end parts deposited with the standard mode of CMT ($WFS_s=7.5$ m/min, $TS_s=13$ mm/s, the geometry scanned is shown in Fig. 3), where the E_m of the W and H are respectively 5.81% and 11.09% at the beginning part, and 4.20% and 18.00% at the end part. It can be noted that for both parts, the irregularity of the height is more significant than that of the width: the width has a larger area of stability ($Y \in [5, 98.5]$ for the presented case), and the end part's width is already very stable ($E_{m-W} < 5\%$) while the crater at the end part results in the most severe height error ($E_{m-H} > 15\%$).

4.1 Performance of the special 2-step mode of CMT

The experimental results indicate that the special 2-step mode of CMT can not increase the geometric accuracy of the bead at the beginning part, but instead aggravated the geometric irregularities. All 16 combinations of parameters ($I_b - t_b$) produce larger E_m in both W and H than the bead deposited with the standard mode of CMT. Figure 9-1a presents one of them deposited by $I_b=135\%$ and $t_b=0.5$ s, where the E_m of the W and H are 7.36% and 12.27%. The special 2-step mode improves the wetting at the beginning part because of its higher current, meanwhile, the higher current also brings higher melting rate of the wire and makes more material get deposited, thus causing the material accumulation to become more severe.

At the end part, the special 2-step mode is demonstrated to be able to increase the regularity of the bead height: the best result $E_{m-H}=11.25\%$ is obtained by the combination $I_e=65\%$ and $t_e=0.6$ s (shown in Fig. 9-1b). However, since this mode starts to operate only after the torch arrives at the end of the path, the deposited material is gathered at the final point of the deposition ($Y = 100$) and does not uniformly fill the crater along the direction of the length of the bead, thus the width of the end is considerably increased and the resulting irregularity in the width becomes worse than for the standard mode, $E_{m-W}=9.44\%$ for the bead in Fig. 9-1b.

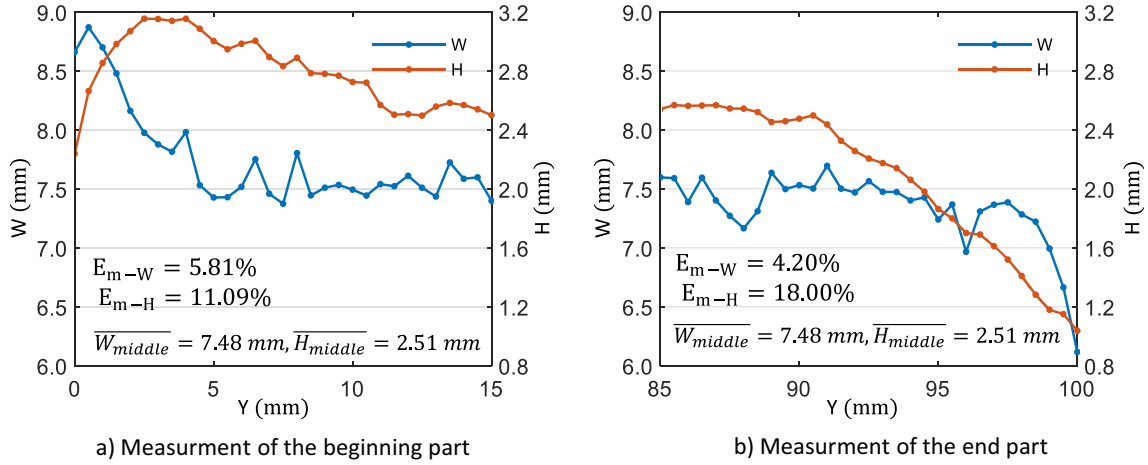


Fig. 8 Measurement of the beginning and end parts of the bead deposited with the standard mode of CMT ($WFS_s=7.5$ m/min, $TS_s=13$ mm/s)

4.2 Performance of the varying TS configurations

According to the experimental results, the torch's acceleration within the beginning part effectively reduces the material accumulation: the most regular geometry is obtained by the parameters $TS_{b1}=130\%$, $TS_{b2}=120\%$, and $TS_{b3}=110\%$, which was therefore chosen as part of the improvement strategy for the beginning part of the bead. Figure 9-2a presents the improved beginning part: the E_m of W and H are decreased to 3.92% and 4.85%, respectively.

Nevertheless, at the end part, the varying TS configurations do not increase the bead geometric accuracy as well as at the beginning part. Among the experiments, the resulting geometries of the end part of the bead are similar to those achieved in the special 2-step mode: the material is overly gathered due to the lower TS, thus leading to the over-width of the end part of the bead, while the compensation for the height is not sufficient. One example of the described geometry is shown in Fig. 9-2b for the end part compensated with $TS_{e1}=75\%$, $TS_{e2}=50\%$, and $TS_{e3}=25\%$, where E_{m-H} is improved to 10.62% but the E_{m-W} is increased to 9.09%.

4.3 Performance of the extra return path

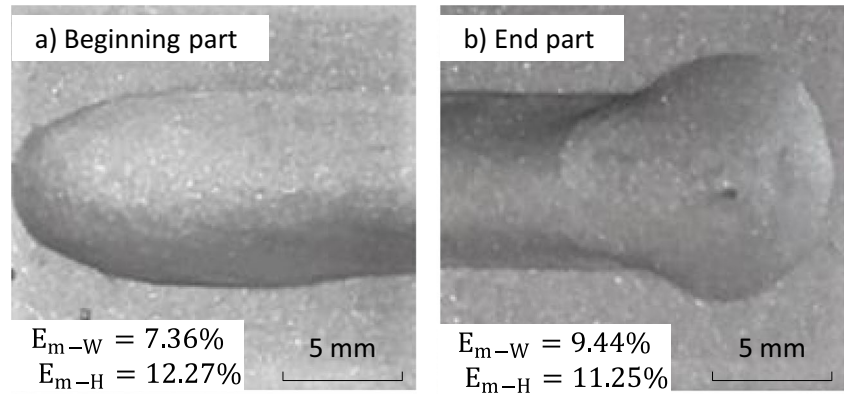
On the basis of the experiments conducted, the extra return path is able to significantly enhance the geometric accuracy at the end part of the bead. Among all the 16 combinations of parameters tested, the optimal improvement is obtained by $TS_r=120\%$ and $WFS_r=70\%$. Figure 9-3a presents the geometry realized: E_m of H is decreased to 7.05% while the width is kept stable ($E_{m-W}=4.58\%$). Through the proposed method, the crater at the end of the bead is filled uniformly: the higher TS and lower WFS reduce both the deposition rate and the heat input, thus ensuring a stable geometry. However, the area near the end of the

torch's return path is still found to be slightly lower and narrower than the stable middle part (example circled in red in Fig. 9-3a) in the experiments. Extra experiments were carried out to resolve this problem by adding an arc holding time: when the torch reaches the end of the return path, instead of being extinguished immediately, the arc is kept on for an additional 0.9 s to fill in more material (The value of 0.9 s is determined by extra experiments, which makes the best compensation for the target area). The resulting end part is shown in Fig. 9-3b, where the regularity of the height is further enhanced to $E_{m-H}=5.38\%$ and a stabler width is achieved ($E_{m-W}=3.26\%$). Thus, this method with its optimal configuration identified is included in the improvement strategy for the end part of the bead.

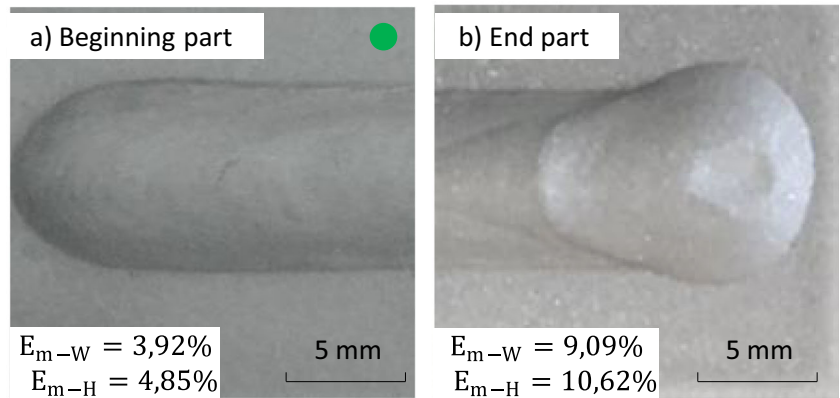
4.4 Validation tests of the developed improvement strategy

The improvement strategy (illustrated in Fig. 7) is developed by combining the two best methods in increasing the geometric accuracy respectively for the bead's beginning part (Fig. 9-2a) and for the bead's end part (Fig. 9-3b). Figure 10 shows the measurement results of the beginning and end parts of the bead deposited with the developed improvement strategy. The standard WFS and TS of the deposition have been also set to the same values as the bead deposited with only the standard mode of the CMT. Compared to the measurement results shown in Fig. 8, at the beginning part, the strategy effectively reduces the maxima of the W and H and enhances the dimensional stability: E_{m-W} and E_{m-H} are decreased to 3.64% and 5.06% while the corresponding values are 5.81% and 11.09% in the deposition without improvement. At the end part, the crater is almost filled to a flat surface (E_{m-H} dropped from 18.00 to 4.89%) while the regularity of the width is maintained

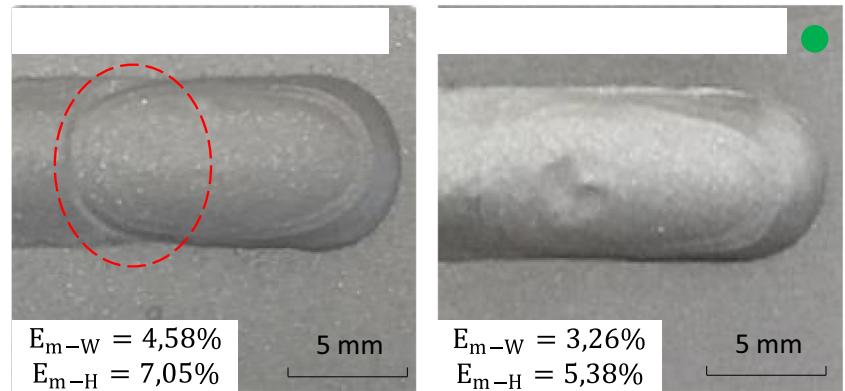
Fig. 9 Improvements yielded by the three different methods tested



1. CMT special 2-step mode



2. Varying TS configurations



3. Extra return path for the end parts

(E_{m-W} is respectively 3.71% and 4.20% for the deposition with and without the improvement strategy).

During the development of the strategy, the standard process parameters were fixed ($WFS_s = 7.5$ m/min and $TS_s = 13$ mm/s). Therefore, more experiments were conducted to test the strategy's robustness by depositing single beads with different combinations of WFS_s and TS_s . Table 5 shows the experimental data of these tests. The values of WFS_s were set to lie within the range of [6.5, 10.0]

(m/min) and the TS_s was varied within [10.00, 16.66] (mm/s). The limits of the WFS_s and TS_s are determined by preliminary experiments for ensuring stable deposition of beads. As the actual WFS varies from its set value, the $\overline{WFS_s}$ and $\overline{I_s}$ represent the mean values of the measured WFS and current of the standard mode, the measurement is provided by the welding source. Figure 11 gives the E_m of W and H at the beginning and end parts of the different beads deposited in the tests. It can be noted that

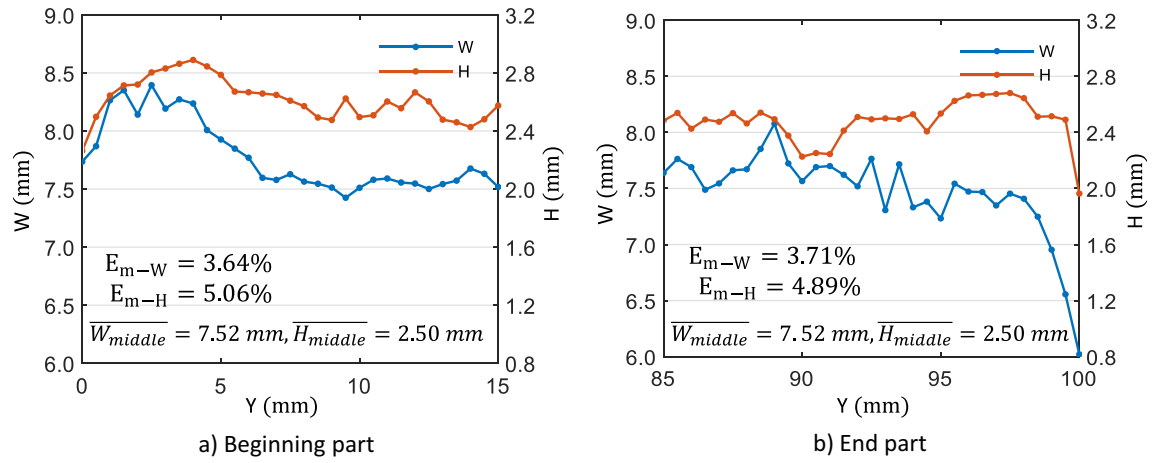


Fig. 10 Measurement of the beginning and end parts of the bead deposited with the improvement strategy ($WFS_s=7.5$ m/min, $TS_s=13$ mm/s)

Table 5 Experimental data for testing the developed improvement strategy

	No. test	1	2	3	4	5	6	7	8	9	10	11	12
Values set	WFS_s (m/min)	6.5	6.5	6.5	7.5	7.5	7.5	9.0	9.0	9.0	10.0	10.0	10.0
	TS_s (mm/s)	10.00	13.33	16.66	10.00	13.33	16.66	10.00	13.33	16.66	10.00	13.33	16.66
Values measured	$\overline{WFS_s}$ (m/min)	6.3	6.2	6.3	7.7	7.7	7.6	9.0	9.1	9.3	10.2	10.1	10.2
	$\overline{I_s}$ (A)	194	188	194	233	233	230	259	261	263	284	281	283

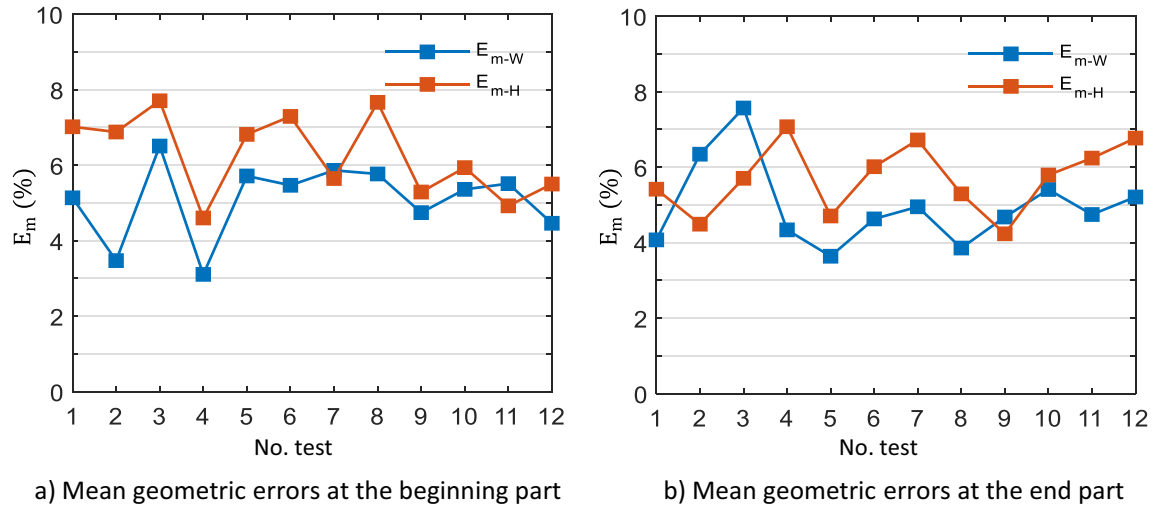


Fig. 11 Tests of the robustness of the developed improvement strategy with different parameters from Table 5

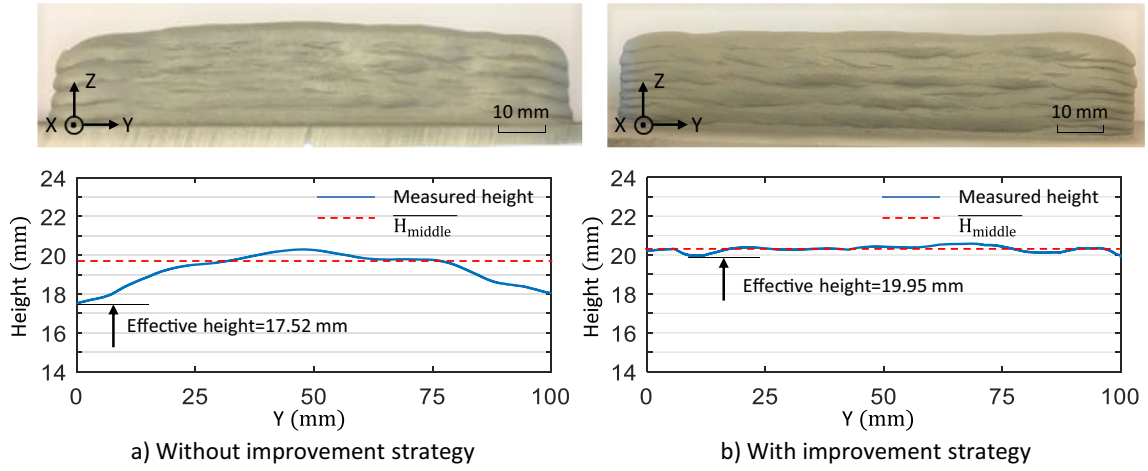


Fig. 12 Thin-wall parts and the corresponding height measurements

the improvement strategy ensures dimensional stability at both the beginning and end parts of the beads (maximum $E_m < 8\%$ for both W and H), thus improving the overall geometric accuracy. While maintaining the bead width stable at the beginning and end parts, the developed strategy is demonstrated to be effective in reducing the geometric irregularity of the bead's height, particularly at the end part: the maximum E_{m-H} is less than 7.1% due to the uniform filling of the crater. Therefore the developed improvement strategy is demonstrated to be robust and seems to be suitable for all process parameters of the single bead's deposition.

4.5 Applications of the improvement strategy

In the fabrication of thin-wall (single-bead multi-layer) parts by WAAM, the height deviation caused by the ignition and extinction of the arc at the two ends of the part needs to be eliminated [12]. As illustrated in [23], an alternating direction path (adjacent layers are deposited in opposite directions) is employed to make the hump at the beginning part and the crater at the end part compensate for each other. With the standard mode of the CMT set at $WFS_s=7.5$ m/min and $TS_s=13.00$ mm/s, a 10-layer thin-wall part was manufactured using an alternating direction

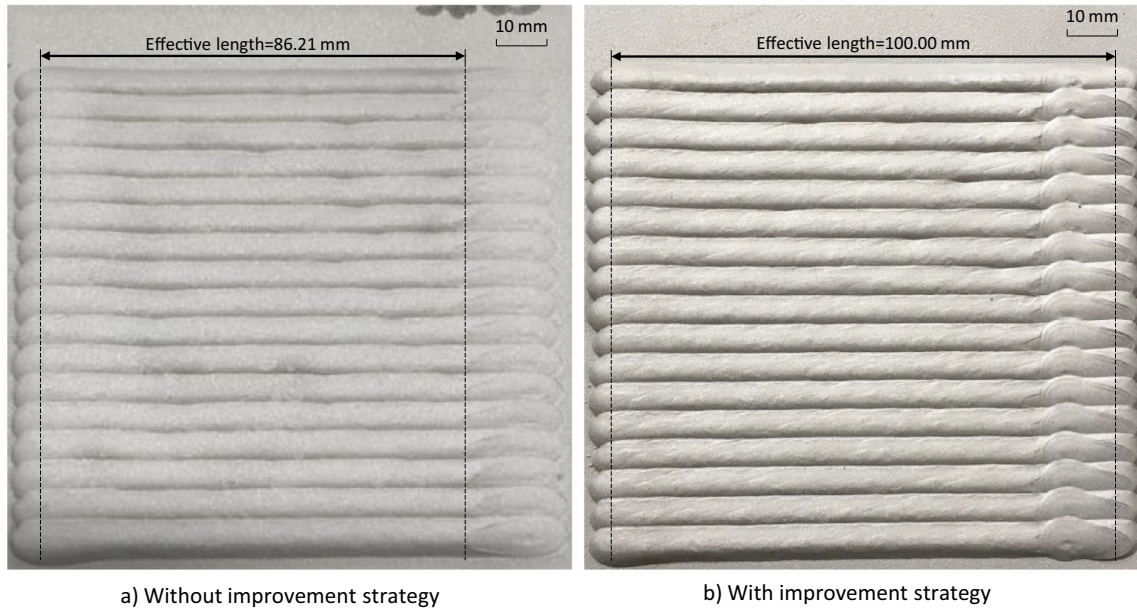


Fig. 13 Multi-pass claddings with deposition length of 100 mm

path, the deposition length being 100 mm for each layer. However, as presented in Fig. 12(a), this method can not improve the height errors very well at the two ends of the wall. Both ends are lower than the middle part due to the accumulated craters at the end of the beads, which are not fully compensated for. Compared to the mean height of the middle part ($\overline{H_{middle}}$), the part's maximum absolute deviation of the height is more than 2.2 mm at the edge. The effective height of the wall (determined by the minimum height in the deposition length) is 17.52 mm. With the same deposition path and parameters, another thin-wall part was deposited using the improvement strategy. Figure 12b shows the part and the corresponding height measurement. It can be observed that the height deviations at the two ends are significantly reduced: the maximum absolute height deviation is smaller than 0.9 mm and the effective height is increased to 19.95 mm. Therefore, it can be confirmed that the accuracy of the geometry of the thin-wall part is improved by employing the strategy at the beginning and end parts of the beads.

The improvement strategy was also applied in multi-pass cladding, where a consistent bead geometry should be maintained [24]. With $WFS_s=9$ m/min and $TS_s=13.33$ mm/s, a 17-pass cladding was manufactured by the standard mode of the CMT: each pass was deposited in the same direction, and the deposition length was fixed at 100 mm. Figure 13a shows the resulting cladding. A stable geometry was achieved in the first 86.21 mm of the cladding, but the end part can not be considered as an effective cladding due to the lower and irregular cladding height. Then the same cladding was deposited with the improvement strategy, this is presented in Fig. 13b: the end part of the cladding is uniformly compensated to enhance the stability of the height, thus a regular geometry is obtained over the whole length of the deposition.

It should be noticed that the developed strategy has not been applied to other material (wire and substrate), which could be a good point of the future work.

5 Conclusions

An improvement strategy was developed to deal with the geometric irregularities at the beginning and end parts of the bead in cold metal transfer (CMT)-based wire-arc additive manufacturing (WAAM). Based on experimental tests, the improvement of the geometric accuracy has been verified on single beads, a thin-wall part, and a multi-pass cladding with the same strategy. The following conclusions can be drawn:

In the standard mode of CMT, compared to the stable geometry at the middle part of the bead, the geometric errors of the height at both the beginning and end parts ($> 11\%$) are more significant than the geometric errors of the width

($< 6\%$); the end part's height error is particularly severe ($= 18\%$ in the presented case).

The experimental results indicate that a special 2-step mode of CMT can not help enhance the dimensional stability at the beginning and end parts of the bead. But in the developed strategy, a gradual decrease of the travel speed (TS) from a higher value is adopted at the beginning part of the bead, and an extra return path with an additional arc holding time is taken to improve the geometry at the end part of the bead. The integration of the CMT process with an industrial robot makes the control of the TS and path in the improvement strategy more accurate and convenient.

The improvement strategy has been tested in the deposition of single beads with different combinations of the process parameters. The strategy is found to be able to ensure dimensional stability at both the beginning and end parts of the different beads (maximum geometric error $< 8\%$ for both width and height), the end part's height errors are limited to less than 7.1%.

The improvement strategy was also applied to the manufacturing of a thin-wall part and a multi-pass cladding. The measurement data in experiments has shown that the geometric accuracy is improved in both cases.

Acknowledgements The authors would like to thank M. Sylvio de Paolis and M. Daniel Boehm for their support and investment during the experimental work, as well as the CPER (State-Region contract) Cyber-Enterprises and the Grand Est Region funding plans.

Declarations

Conflict of interest The authors declare no competing interests.

References

1. Pan Z, Ding D, Wu B, Cuiuri D, Li H, Norrish J (2018) Arc Welding Processes for Additive Manufacturing: A Review. In: Transactions on Intelligent Welding Manufacturing. Springer Singapore, pp 3–24, https://doi.org/10.1007/978-981-10-5355-9_1
2. Liu J, Xu Y, Ge Y, Hou Z, Chen S (2020) Wire and arc additive manufacturing of metal components: A review of recent research developments. International Journal of Advanced Manufacturing Technology. <https://doi.org/10.1007/s00170-020-05966-8>
3. Selvi S, Vishvakshenan A, Rajasekar E (2018) Cold metal transfer (CMT) technology - An overview. Defence Technology. <https://doi.org/10.1016/j.dt.2017.08.002>
4. Sun Z, Lv Y, Xu B, Liu Y, Lin J, Wang K (2015) Investigation of droplet transfer behaviours in cold metal transfer (CMT) process on welding Ti-6Al-4V alloy. International Journal of Advanced Manufacturing Technology. <https://doi.org/10.1007/s00170-015-7197-9>
5. Frostevarg J, Kaplan AF, Lamas J (2014) Comparison of CMT with other arc modes for laser-arc hybrid welding of steel. Welding in the World. <https://doi.org/10.1007/s40194-014-0146-7>
6. Ayarkwa K, Williams S, Ding J (2015) Investigation of pulse advance cold metal transfer on aluminium wire arc additive man-

- ufacturing. *Int J Rapid Manuf* 5(1):44. <https://doi.org/10.1504/ijrapidm.2015.073547>
7. Ali Y, Henckell P, Hildebrand J, Reimann J, Bergmann JP, Barnikol-Oettler S (2019) Wire arc additive manufacturing of hot work tool steel with CMT process. *J Mater Process Technol* 269. <https://doi.org/10.1016/j.jmatprotec.2019.01.034>
8. Zinke M, Burger S, Arnhold J, Jüttner S (2021) Effect of different variants of filler metal S Ni 6625 on properties and microstructure by additive layer manufactured using CMT process. *Welding in the World*. <https://doi.org/10.1007/s40194-021-01105-3>
9. Ding D, Pan Z, Cuiuri D, Li H (2015) Wire-feed additive manufacturing of metal components: Technologies, developments and future interests. *Int J Adv Manuf Technol* 81(1–4):465–481. <https://doi.org/10.1007/s00170-015-7077-3>
10. Kozamernik N, Bračun D, Klobčar D (2020) WAAM system with interpass temperature control and forced cooling for near-net-shape printing of small metal components. *International Journal of Advanced Manufacturing Technology*. <https://doi.org/10.1007/s00170-020-05958-8>
11. Kwak YM, Doumanidis CC (2002) Geometry regulation of material deposition in near-net shape manufacturing by thermally scanned welding. *J Manuf Process* 4(1):28–41. [https://doi.org/10.1016/S1526-6125\(02\)70131-X](https://doi.org/10.1016/S1526-6125(02)70131-X)
12. Xiong J, Zhang G (2014) Adaptive control of deposited height in GMAW-based layer additive manufacturing. *J Mater Process Technol* 214(4):962–968. <https://doi.org/10.1016/j.jmatprotec.2013.11.014>
13. Zhao Y, Li F, Chen S, Lu Z (2019) Unit block-based process planning strategy of WAAM for complex shell-shaped component. *International Journal of Advanced Manufacturing Technology*. <https://doi.org/10.1007/s00170-019-04141-y>
14. Karunakaran KP, Suryakumar S, Pushpa V, Akula S (2010) Low cost integration of additive and subtractive processes for hybrid layered manufacturing. *Robotics and Computer-Integrated Manufacturing*. <https://doi.org/10.1016/j.rcim.2010.03.008>
15. Zhang YM, Chen Y, Li P, Male AT (2003) Weld deposition-based rapid prototyping: a preliminary study. *J Mater Process Technol* 135(2–3 SPEC.):347–357. [https://doi.org/10.1016/S0924-0136\(02\)00867-1](https://doi.org/10.1016/S0924-0136(02)00867-1)
16. Xia C, Pan Z, Polden J, Li H, Xu Y, Chen S, Zhang Y (2020) A review on wire arc additive manufacturing: Monitoring, control and a framework of automated system. <https://doi.org/10.1016/j.jmsy.2020.08.008>
17. Hu S, Zhang H, Wang Z, Liang Y, Liu Y (2016) The arc characteristics of cold metal transfer welding with AZ31 magnesium alloy wire. *Journal of Manufacturing Processes*. <https://doi.org/10.1016/j.jmapro.2016.10.001>
18. Ding D, Shen C, Pan Z, Cuiuri D, Li H, Larkin N, Van Duin S (2016) Towards an automated robotic arc-welding-based additive manufacturing system from CAD to finished part. *CAD Comput Aided Des* 73:66–75. <https://doi.org/10.1016/j.cad.2015.12.003>
19. Xiong J, Zhang G, Qiu Z, Li Y (2013) Vision-sensing and bead width control of a single-bead multi-layer part: Material and energy savings in GMAW-based rapid manufacturing. *J Clean Prod* 41:82–88. <https://doi.org/10.1016/j.jclepro.2012.10.009>
20. Heralić A, Christiansson AK, Ottosson M, Lennartson B (2010) Increased stability in laser metal wire deposition through feedback from optical measurements. *Opt Lasers Eng* 48(4):478–485. <https://doi.org/10.1016/j.optlaseng.2009.08.012>
21. Guo H, Hu J, Tsai HL (2009) Formation of weld crater in GMAW of aluminum alloys. *International Journal of Heat and Mass Transfer*. <https://doi.org/10.1016/j.ijheatmasstransfer.2009.06.028>
22. Xia C, Pan Z, Zhang S, Li H, Xu Y, Chen S (2020) Model-free adaptive iterative learning control of melt pool width in wire arc additive manufacturing. *International Journal of Advanced Manufacturing Technology*. <https://doi.org/10.1007/s00170-020-05998-0>
23. Ma G, Zhao G, Li Z, Yang M, Xiao W (2019) Optimization strategies for robotic additive and subtractive manufacturing of large and high thin-walled aluminum structures. *International Journal of Advanced Manufacturing Technology*. <https://doi.org/10.1007/s00170-018-3009-3>
24. Pickin CG, Williams SW, Lunt M (2011) Characterisation of the cold metal transfer (CMT) process and its application for low dilution cladding. *Journal of Materials Processing Technology*. <https://doi.org/10.1016/j.jmatprotec.2010.11.005>

Publisher's note Springer Nature remains neutral with regard to jurisdictional claims in published maps and institutional affiliations.